BIOCHEMISTRY

Self-limiting multimerization of α-synuclein on membrane and its implication in Parkinson's diseases

Dong-Fei Ma[1]†, Shenqing Zhang[2,3]†, Si-Yao Xu[1,4]†, Zi Huang[1,4], Yuanxiao Tao[5,6], Feiyang Chen[2,3], Shengnan Zhang[7,8], Dan Li[2,3], Tongsheng Chen[4], Cong Liu[7,8]*, Ming Li[1,5,6]*, Ying Lu[1,5,6]*

α-Synuclein (α-syn), a crucial molecule in Parkinson's disease (PD), is known for its interaction with lipid membranes, which facilitates vesicle trafficking and modulates its pathological aggregation. Deciphering the complexity of the membrane-binding behavior of α-syn is crucial to understand its functions and the pathology of PD. Here, we used single-molecule imaging to show that α-syn forms multimers on lipid membranes with huge intermultimer distances. The multimers are characterized by self-limiting growth, manifesting in concentration-dependent exchanges of monomers, which are fast at micromolar concentrations and almost stop at nanomolar concentrations. We further uncovered movement patterns of α-syn's occasional trapping on membranes, which may be attributed to sparse lipid packing defects. Mutations such as E46K and E35K may disrupt the limit on the growth, resulting in larger multimers and accelerated amyloid fibril formation. This work emphasizes sophisticated regulation of α-syn multimerization on membranes as a critical underlying factor in the PD pathology.

INTRODUCTION

α-Synuclein (α-syn), an inherently unstructured protein, is principally located at presynaptic terminals within the nervous system (*1*, *2*). Its amphipathic characteristics are crucial for its interaction with lipid membranes (*3*, *4*). Previous studies using solution nuclear magnetic resonance (NMR), solid-state NMR, and electron paramagnetic resonance have demonstrated that the N-terminal region of α-syn is responsible for its membrane binding (*3*, *5*–*9*). Moreover, chemical cross-linking and fluorescence resonance energy transfer (FRET) methods have been used to show that α-syn forms multimer upon binding to the membrane (*10*). However, how α-syn assemblies into multimer on the membrane remains poorly understood at the single-molecule level. Although the exact physiological functions of α-syn remain elusive (*11*–*13*), its role in managing synaptic vesicle dynamics and neurotransmitter release is increasingly recognized, primarily mediated through its interactions with lipids (*14*–*18*). α-Syn is also a key mediator of the pathology of Parkinson's disease (PD) (*19*–*21*), in which abnormally it accumulates as insoluble fibrils (*22*–*30*), contributing to the formation of Lewy bodies in neurons. This aggregation is profoundly affected by the lipid environment (*31*–*34*). For instance, mitochondrial membrane has been shown to accelerate the pathological aggregation of α-syn (*35*–*37*). In addition, PD is characterized by substantial changes in brain lipid metabolism and composition (*38*–*41*), indicating that there is a strong link between α-syn misfolding and disruptions in lipid balance. Moreover, disease-causing mutation E46K within the N-terminal region of α-syn alters its membrane-binding property (*42*), highlighting the importance of α-syn–membrane interplay in mediating its function and pathology.

α-Syn is carried between cells by exocellular vesicles (*43*–*45*), and those with surface-bound α-syn are more likely to be internalized (*43*). The extracellular concentration of α-syn is extremely low, typically in the nanomolar scale (*46*), suggesting that the surface-bound α-syn must engage in strong interactions with lipid membranes to achieve stable attachment. On the other hand, α-syn also functions in intracellular regions where concentration of α-syn is estimated to be approximately 35 to 70 μM (*46*). In the presence of such high concentration, the potent membrane binding of α-syn would be expected to cause a vast accumulation of the protein on cellular membranes, potentially disrupting the integrity of presynaptic terminals and synaptic vesicles. However, how one protein can similarly interact with lipid membranes in two extremely different environments is not clear.

Single-molecule imaging permits the direct observation of stochastic, dynamic processes involving individual molecules in real time, in contrast to ensemble methods. It has been previously used to investigate not only α-syn (*18*) but also other membrane-interacting proteins, for example, G protein–coupled receptors (*47*, *48*), soluble *N*-ethylmaleimide–sensitive factor attachment protein receptors (*49*), and the mixed-lineage kinase domain-like protein (*50*). The significant advance in the analysis of membrane proteins that is provided by single-molecule methods is the ability to analyze signals associated with conformational states, without the need to sort the molecular populations (*51*). This permits greater understanding of the physiological functions or pathology associated with membrane proteins. In the present study, we used single-molecule imaging to characterize the interaction of α-syn with negatively charged lipid bilayers. We show that α-syn does not accumulate in large quantities on liposome when present at high concentrations, and it does not completely disassociate from lipid bilayers even after removing free α-syn in the buffer. This binding is characterized by a self-limiting multimerization process, which involves the dynamic exchange of

[1]Songshan Lake Materials Laboratory, Dongguan, Guangdong 523808, China. [2]Bio-X Institutes, Key Laboratory for the Genetics of Developmental and Neuropsychiatric Disorders (Ministry of Education), Shanghai Jiao Tong University, Shanghai 200030, China. [3]Zhangjiang Institute for Advanced Study, Shanghai Jiao Tong University, Shanghai 200240, China. [4]MOE & Guangdong Key Laboratory of Laser Life Science, College of Biophotonics, South China Normal University, Guangzhou, Guangdong, China. [5]Beijing National Laboratory for Condensed Matter Physics, Institute of Physics, Chinese Academy of Sciences, Beijing 100190, China. [6]University of Chinese Academy of Sciences, Beijing 100049, China. [7]Interdisciplinary Research Center on Biology and Chemistry, Shanghai Institute of Organic Chemistry, Chinese Academy of Sciences, Shanghai 201210, China. [8]State Key Laboratory of Chemical Biology, Shanghai Institute of Organic Chemistry, Chinese Academy of Sciences, Shanghai 200032, China.
*Corresponding author. Email: liulab@sioc.ac.cn (C.L.); mingli@iphy.ac.cn (M.L.); yinglu@iphy.ac.cn (Y.L.)
†These authors contributed equally to this work.

monomers and is impeded in large areas surrounding the multimers. Moreover, both the mutations of E46K and E35K cause α-syn to form larger multimers on membrane and increase its propensity to amyloid fibrillization. These findings demonstrate the self-limiting adsorption and multimerization behavior of α-syn on membrane and thereby not only improve our understanding of the organization and vesicular transmission of α-syn between cells but also shed light on its involvement in the pathology of PD.

RESULTS

Limited adsorption but strong post-binding retention of α-syn on liposomes

We used total internal reflection fluorescence (TIRF) microscopy to evaluate the adsorption of α-syn onto liposomes at various α-syn concentrations. The incident angle of the light was adjusted to ensure a sufficient penetration depth of the evanescent field. We sequentially added 5 nM and then increased to 50 nM Alexa Fluor 555–labeled α-syn (α-syn T72C–Alexa 555) to 200-nm liposomes, composed of 10% 1,2-dioleoyl-*sn*-glycero-3-phosphate (DOPA) and 90% 1,2-dioleoyl-*sn*-glycero-3-phosphocholine (DOPC) (molar ratio), which were anchored to a polyethylene glycol (PEG)–passivated surface, with intervening washes with buffer. After each addition and wash, the samples were incubated for 10 min before each observation (Fig. 1A). Intriguingly, compared with the 5 nM α-syn concentration, there were only moderate increases in the amount of α-syn on liposomes when the 50 nM α-syn concentration was added (Fig. 1, A to C). After rinsing with buffer solution, there was a substantial reduction in the α-syn adsorption. Moreover, once the concentration of α-syn was increased to 200 nM, the adsorption after washing with buffer stabilized at a level similar to that after the wash following the addition of the 50 nM concentration within 10 min (fig. S1). We calculated that approximately six monomers were associated with each liposome at 50 nM (Fig. 1C, data corrected for the labeling rate), decreasing to approximately three to four monomers within 10 min after washing with buffer (Fig. 1D). This implies that α-syn does not fully occupy the liposome surface, even when present at high concentrations (*52*) (details in Supplementary Text).

After removing the free α-syn from the solution, we analyzed changes in the number of liposomes bound with α-syn over time to characterize the protein's retention on membranes. Notably, the number of liposomes occupied by α-syn decreased very slowly, with a decay constant of ~264 min, suggesting a very slow dissociation process (Fig. 1E). It is unusual that α-syn neither rapidly disassociates from membranes in the absence of a supply of protein nor accumulates in large amounts on the membrane when a high concentration of protein is present in the buffer.

Sparse, size-limited α-syn multimers on SLB

To further characterize the limited membrane absorption of α-syn, we used supported lipid bilayers (SLBs), in place of liposomes, to directly monitor the assembly of α-syn because liposomes have diameters below the diffraction limit for optical imaging. α-Syn T72C–Alexa 555 was incubated on SLBs for 10 min at concentrations of 5 or 50 nM, and images were acquired by TIRF, with the intensity of spots corresponding to α-syn multimers being normalized to the intensity associated with a single α-syn monomer (Fig. 2, A to C). This showed that α-syn forms multimers comprising of three to four monomers at 5 nM and approximately six monomers at 50 nM (Fig. 2D). Multimers comprising two to four monomers also formed at a 0.5 nM concentration of α-syn if the incubation was sufficiently long (fig. S2). Remarkably, after washing following the addition of the 50 nM sample (Fig. 2C), the size of the α-syn multimer decreased to three to four monomers, which was similar to the size of the α-syn multimer formed at the 5 nM concentration (Fig. 2A). These data suggest that there is limited absorption and multimerization of α-syn upon its binding to lipid bilayers.

Notably, we found large, protein-free areas surrounding the multimers on the SLB surface, with mean areas of approximately 0.6 μm^2 at both concentrations (Fig. 2E). This intermultimer space persisted after washing, implying that α-syn multimers do not readily dissociate from the membrane. Moreover, the areas around these multimers were larger than the surface area of a 200-nm liposome (~0.13 μm^2), suggesting that α-syn likely forms a single multimer per liposome.

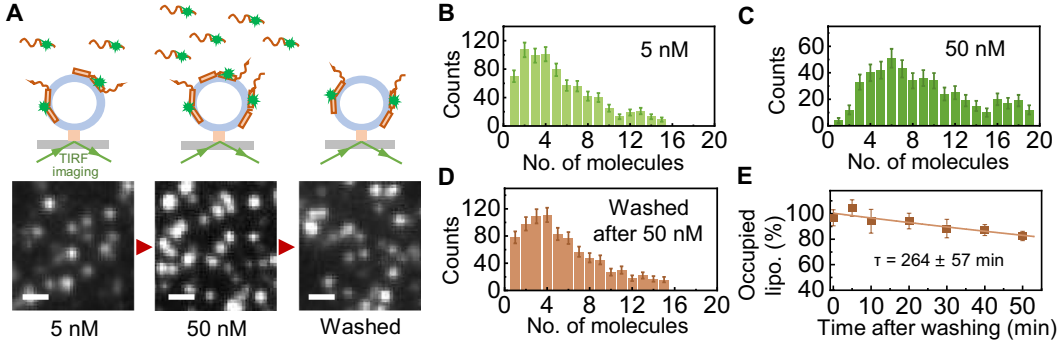

Fig. 1. Limited adsorption of α-syn onto 200-nm liposomes. (**A**) Adsorption of α-syn T72C–Alexa 555 onto 200-nm liposomes anchored on a glass surface, observed by TIRF imaging, as the protein concentration was increased from 5 to 50 nM, followed by a phosphate-buffered wash. The incident angle of the light was adjusted to permit a sufficient penetration in the evanescent field. Scale bars, 1 μm. (**B** to **D**) Mean number of proteins on individual liposomes calculated using the fluorescent intensity. Each histogram was built from >500 spots. The error bars represent the statistical error. (**E**) Quantitative analysis of the change in the amount of the liposomes occupied by α-syn after the removal of free proteins in the solution. The relative counts of the fluorescence spots in the image that represents the amount of the liposomes with bound α-syn were calculated over time. The characteristic time τ was derived from the single-exponential fitting.

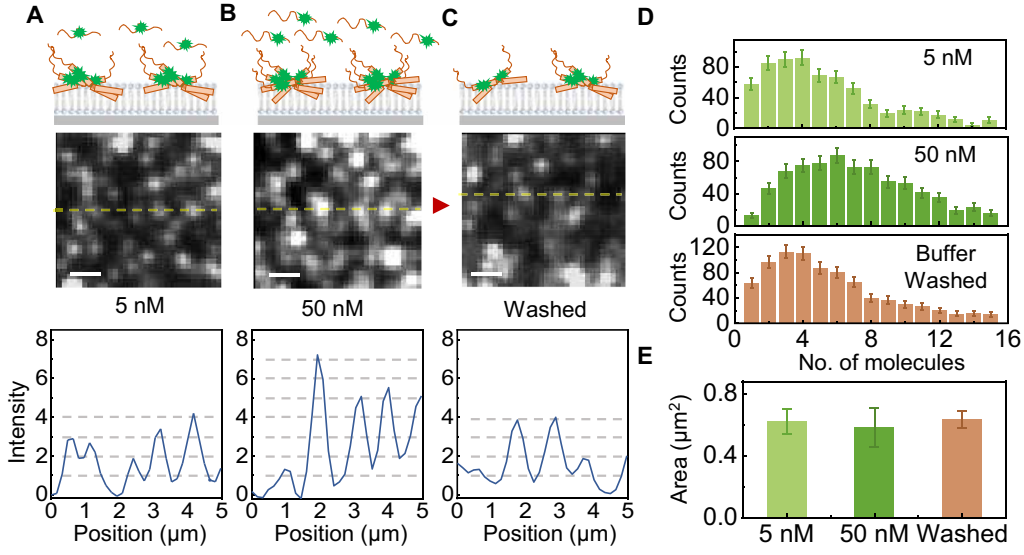

Fig. 2. α-Syn multimers are formed on SLBs. (**A** to **C**) TIRF images (middle) and intensity profiles along the specified lines (bottom), following the addition of 5 nM (A) and 50 nM (B) α-syn T72C–Alexa 555 and a subsequent 10-min incubation. The image in (C) was obtained after wash with buffer followed by 10-min incubation in the 50 nM channel. Scale bars, 1 μm. The cartoon on top of each set depicts the state of α-syn on SLB. (**D**) Statistics analysis of the multimer sizes observed in (A) to (C). The size is quantified as the number of molecules. Each histogram was built from >500 spots. (**E**) Calculated mean area around single multimers in (A) to (C).

Occasional trapping of α-syn on membrane surfaces

To further characterize the diffusion pattern of α-syn and its multimerization on lipid membranes, we simultaneously tracked the real-time trajectories of monomers or multimers by monitoring the fluorescence traces. Initially, we observed the landing and diffusion of monomers following the introduction of 1 nM α-syn into the system. The movement of α-syn displayed unique characteristics, which differed from standard Brownian motion and featured a mix of unrestricted diffusion with occasional local entrapment as seen in the trajectories in Fig. 3A. We then explored how these trapping events influence the membrane binding of α-syn. Proteins encountering these traps exhibited two distinct step sizes at 0.5-s intervals (Fig. 3B, top) and a longer mean dwell time of 17 s on the membrane, which was limited by the extent of photobleaching under the experimental conditions used (Fig. 3B, bottom). This was significantly longer than the ~2.2-s dwell time for proteins not caught in the local traps (fig. S3), indicating that these local traps substantially enhance the interactions between α-syn and membrane.

After increasing the concentration of α-syn to 50 nM, we monitored the behavior of both monomers and multimers on the membranes. This revealed two distinct types of movement pattern. The trajectories and step size distribution of the brighter spots suggested that the multimers were immobilized at the trapping sites and did not migrate across the membrane (Fig. 3C and the top in Fig. 3D). In contrast, in the areas surrounding these multimers, α-syn primarily followed paths indicative of free diffusion, without the entrapment noted near multimers (the trajectories colored in blue in Fig. 3C, and the top of Fig. 3E). This implies that multimers might be occupying the trapping sites, thereby reducing the binding of nearby monomers by blocking their access to these sites. The dwell time for monomers distant to the multimers was significantly shorter, at approximately 2.0 s (Fig. 3E, bottom). In contrast, the multimer interactions were more stable, with dwell times averaging approximately 32 s (Fig. 3D, bottom), albeit that this was constrained by photobleaching. This difference in dwell time consistent with the hypothesis that the formation of multimers at the trapping sites reduces the likelihood of monomer entrapment.

Our observations indicate that there is a close link between the membrane adsorption of α-syn and the presence of trapping sites. We postulate that the trapping of α-syn during its movement is the result of the irregular arrangements of lipids on membranes. The movements of α-syn into and out of the trapping zones indicate that they are the result of transient fluctuation or topological imperfections in membrane lipid arrangements (*53*–*56*), rather than defects created during lipid bilayer preparation. The occupation of the trapping sites by multimers would reduce the likelihood of monomers being trapped nearby because of weak interactions between the α-syn monomers and defect-free membranes. This results in limited multimer density, dictated by the availability of the trapping sites. In support of this contention, we found that if liposome swells by adjusting osmotic pressure (fig. S4), the adsorption of α-syn onto the liposomes was enhanced. Furthermore, we incorporated cholesterol into liposomes and found that this also promoted liposome binding by α-syn (fig. S5). The incorporation of cholesterol into the membrane was reported to increase the areas of the membrane packing defects (*57*) and may promote the formation of membrane defects that is sufficiently large to accommodate proteins with amphipathic helices (*58*). Our observation further supports the significance of packing defects in α-syn adsorption on the liposome.

Dynamic monomer exchanges in multimers

Next, we sought to monitor the intensities associated with individual multimers on SLBs with time, with the concentrations of α-syn-Alexa 555 in buffer of 50, 5, or 0.5 nM. The intensity traces for these multimers at 50 and 5 nM concentrations displayed frequent,

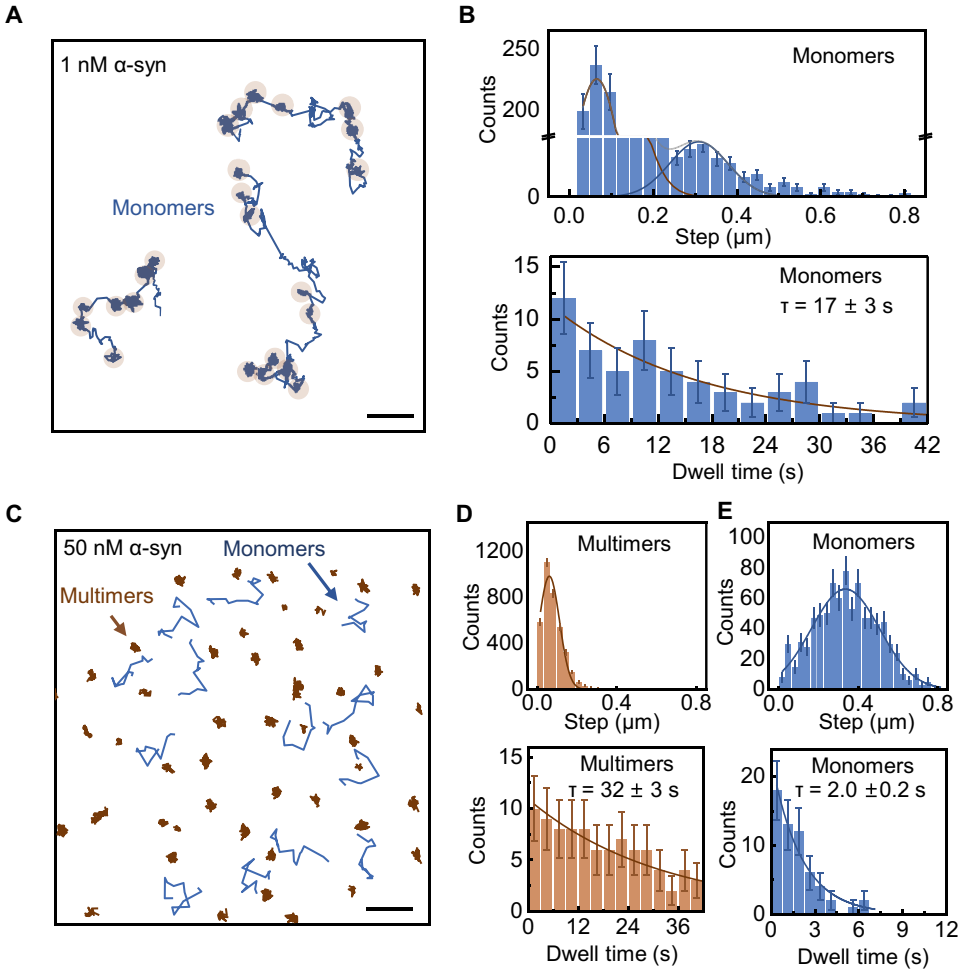

Fig. 3. Entrapment-interspersed motion and correlated multimers of α-syn on lipid bilayers. (**A**) Trajectories of individual α-syn T72C–Alexa 555 (1 nM in solution) on lipid bilayer showing local trappings (marked with shadows in the trajectories). Scale bar, 1 μm. (**B**) Top: Distribution of the displacements in 0.5-s interval building from >1200 moving steps. Bottom: Distribution of the dwell time on lipid bilayer of the proteins with local trappings. The histogram was built from >60 trajectories. (**C**) Multimers formed in 50 nM α-syn T72C–Alexa 555 (brown) and the trajectories of newly landed monomers (blue) adjacent to the multimers. Scale bar, 1 μm. (**D**) Interval step size distribution (0.5-s; top) and the on-membrane dwell times (bottom) of the multimers. The histograms were built from >3000 steps and > 80 traces, respectively (**E**) Interval step size distribution (0.5-s; top) and the on-membrane dwell times (bottom) of the monomers adjacent to the multimers. The histograms were built from >800 steps and >50 traces, respectively.

stepwise fluctuations, that varied according to the concentration (Fig. 4A). These fluctuations imply the dynamic association and dissociation of α-syn monomers with and from the multimers. To discern whether these fluctuations were the result of a transient attachment (kiss-and-run) of a single α-syn monomer or the exchange of monomers with the multimer, we incubated α-syn labeled with Alexa 647 (α-syn T72C–Alexa 647) with SLBs that had been preincubated with α-syn T72C–Alexa 555 multimers (Fig. 4B, top). With alternating excitations by 532- and 640-nm lasers, dual-channel imaging captured temporal evolution of the two differently labeled α-syn. This imaging, in combination with the intensity traces for colocalized Alexa 555 and Alexa 647 (Fig. 4B, bottom left), revealed the replacement of Alexa 555–labeled α-syn in the multimers by α-syn T72C–Alexa 647, demonstrating dynamic monomer exchange between the multimers and the surrounding environment. Consistent with this, examination of the size distribution of the α-syn T72C–Alexa 647 monomers 900 s after their addition indicated that Alexa 647–labeled proteins also assembled into size-limited multimers (Fig. 4B, bottom right). FRET experiments using α-syn T72C–Alexa 555 and α-syn T72C–Alexa 647 also showed that the α-syn T72C–Alexa 647 replaced the α-syn T72C–Alexa 555 in the multimers (fig. S6). It is noteworthy that the fluctuation frequency is apparently lower at lower protein concentrations (Fig. 4A). A count of the number of Alexa 555–positive spots in the images during the replacement by Alexa 647–labeled proteins (Fig. 4C) showed that the displacement rate was higher at higher protein concentrations, and this was confirmed by observing the replacement of membrane-bound α-syn T72C–Alexa 555 by unlabeled proteins (fig. S7). These findings indicate that the sizes of the multimers on the membrane are restricted through a dynamic equilibrium, which limits the absorption of α-syn onto lipid membranes.

Together, these results show that α-syn monomers self-assemble rapidly on membranes to form low-order multimers, as identified following washing (Fig. 2D). The addition of further monomers may

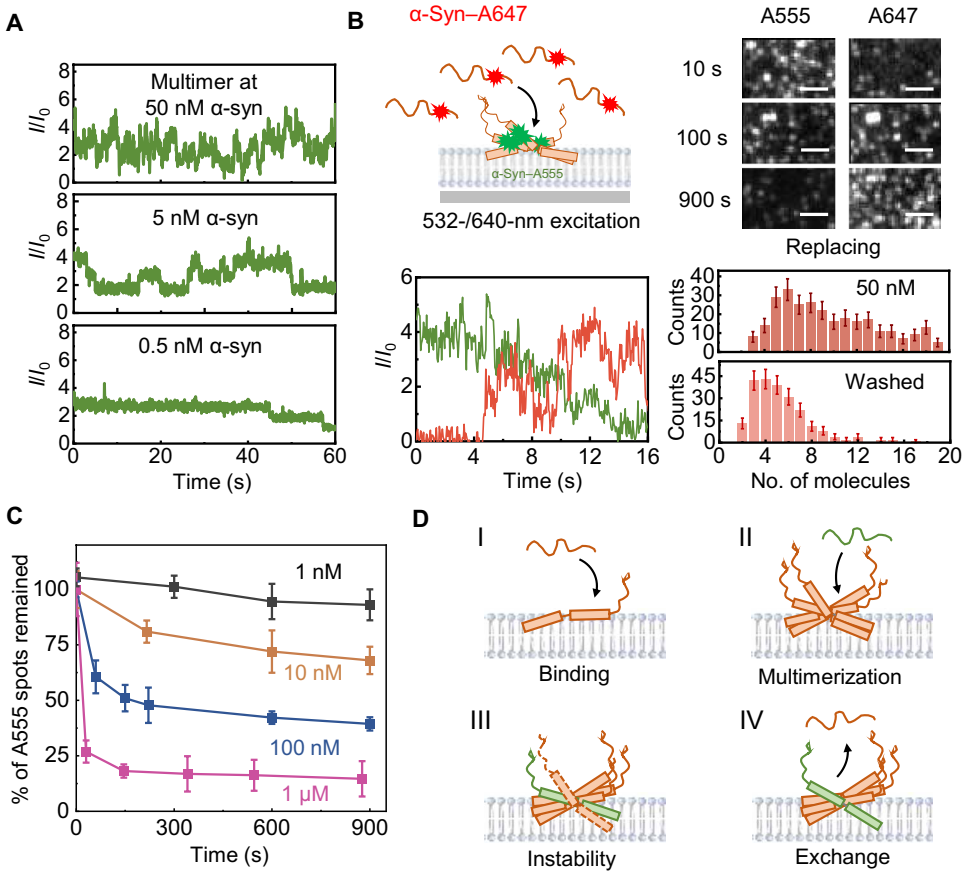

Fig. 4. Exchanges of α-syn in membrane-bound multimers with monomers in solution. (**A**) Representative intensity traces of α-syn multimers at 50, 5, and 0.5 nM α-syn T72C–Alexa 555. (**B**) Top: The scheme (left) and the images (right) of the experiment showing the replacement of α-syn T72C–Alexa 555 by α-syn T72C–Alexa 647 (50 nM) in multimers. The images were taken at the indicated time points after the addition of α-syn T72C–Alexa 647. Scale bars, 1 μm. Bottom left: A representative intensity trace of the α-syn T72C–Alexa 555 multimers (green line) being replaced upon the addition of α-syn T72C–Alexa 647 (red line). Bottom right: The multimer size distribution of the α-syn T72C–Alexa 647 multimers before and after washing with buffer. Each histogram was built from >200 spots. (**C**) Changes of the amount of the α-syn T72C–Alexa 555 multimers upon addition of various concentrations (denoted in the figure) of Alexa 647–labeled α-syn. (**D**) Schematic illustration showing the protein exchange in the multimers.

destabilize these multimers, causing the random release of the proteins and facilitating a dynamic exchange between the multimers and their surroundings (Fig. 4D). This exchange is likely to be the result of an energy barrier that restricts further growth of the multimers.

Formation of larger multimers on membranes and the accelerated aggregation of α-syn mutants

We next aimed to determine whether disease-causing mutation in α-syn might affect the demonstrated self-limiting multimerization by altering its membrane-binding properties. We first investigated the hereditary mutation E46K, which was causative to early-onset familial PD (*59*–*61*) and could influence the membrane binding by α-syn (*42*). To compare the E46K with wild-type (WT) α-syn, we introduced both proteins at concentrations of 50 nM onto SLBs. Intriguingly, we found that although the multimers of the E46K mutant also exhibited monomer exchange (fig. S8), they tended to form larger multimers, comprising approximately 10 to 20 monomers after washing with buffer, in contrast to the WT form (Fig. 5A, middle). This suggests that the E46K mutation disrupts the self-limiting multimerization of α-syn on lipid bilayers, favoring the formation of larger multimers. In addition, we examined another α-syn mutation E35K, which was previously reported to cause dopaminergic neuron loss in rat models (*62*). Similar to E46K α-syn, E35K α-syn formed large multimers on membranes, which were retained after washing with buffer, in contrast to WT α-syn (Fig. 5A, bottom).

In addition, we evaluated the aggregation behaviors of E46K, E35K, and WT α-syn using a thioflavin T (ThT) fluorescence assay (*63*, *64*) in the presence of 200-nm liposomes composed of 10% DOPA and 90% DOPC (molar ratio), with a protein-to-lipid ratio of 1:2.5. Over a 6-day incubation period, all of E46K, E35K, and WT showed accelerated aggregation in the presence of liposomes (Fig. 5B). Compare to WT, the E46K and E35K mutants aggregated faster on the liposomes and formed significantly larger number of amyloid fibrils (Fig. 5, B and C, and fig. S9). These observations imply that both the E46K and E35K mutations disrupt α-syn's self-limiting multimerization, altering the energy landscape of α-syn's confined multimerization on membranes and decreasing the energy barrier for amyloid fibril formation.

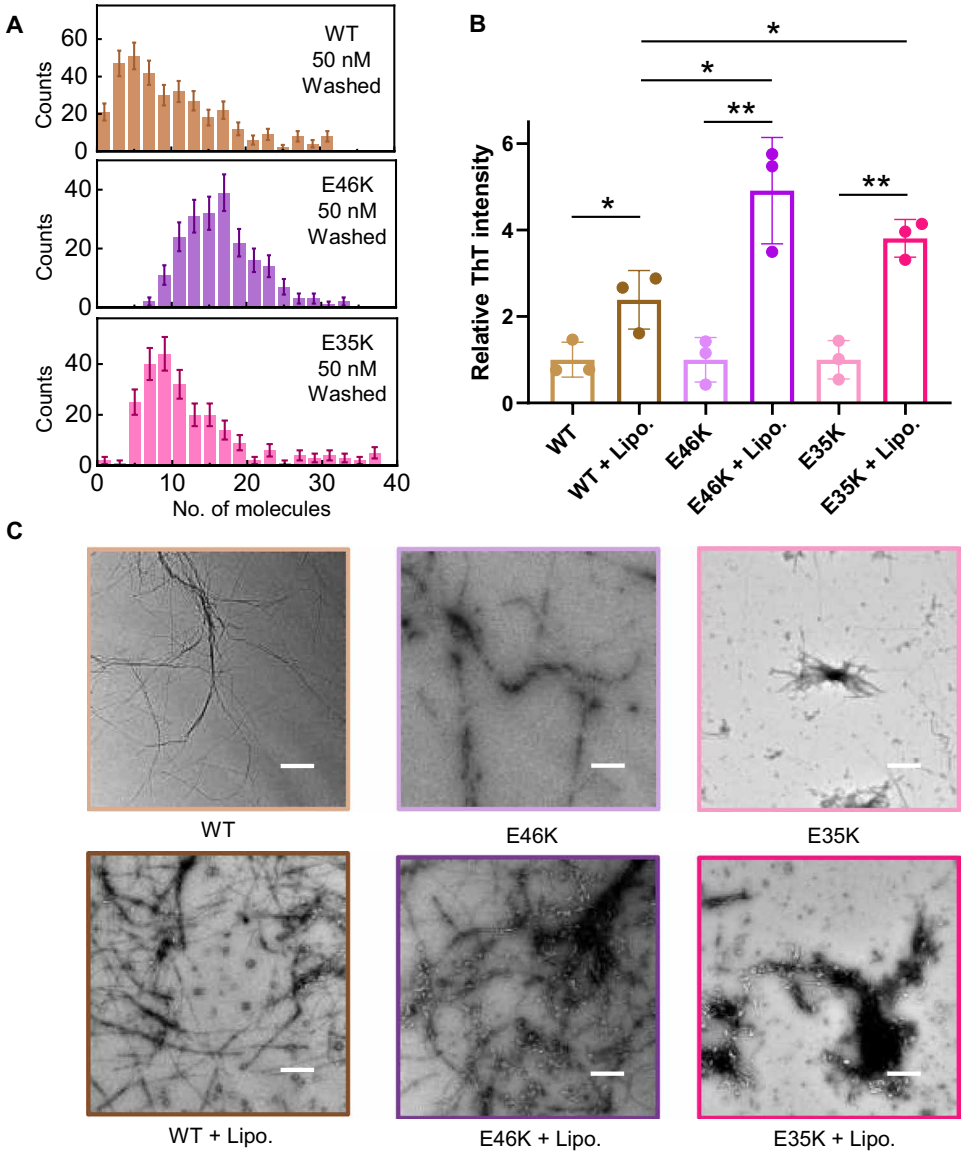

Fig. 5. Membrane-indued multimerization and amyloid aggregation of WT, E46K, and E35K α-syn. (**A**) Size distributions of the multimers on SLB, determined by adding 50 nM protein, incubating for 10 min, rinsing with buffer, and incubating for a further 10 min. Each histogram was built from >200 fluorescent spots. (**B**) Fluorescence intensity of ThT measured from the amyloid aggregate samples of WT, E46K, and E35K, with (protein: liposome = 1: 2.5, molar ratio) and without the liposomes. The ThT fluorescence intensities were normalized to the samples without the liposomes. Data are shown as mean ± SD. $n = 3$. Significance was tested using Student's t test, with $^{*}P < 0.05$ and $^{**}P < 0.01$ indicating statistical significance. (**C**) Representative transmission electron microscopy images taken from the ThT assay as denoted by the colored borders. Scale bars, 1 μm.

DISCUSSION

The present findings illustrate the complex relationship between α-syn and membranes. At low concentrations, α-syn forms stable multimers through a positive cooperative process and show a strong affinity for membranes. Conversely, at high concentrations, the binding within and outside the multimers weakens, leading to reversible and negatively cooperative behavior. This suggests that a concentration-dependent, self-regulatory mechanism affects the interaction between α-syn and membranes. Previous studies have shown that α-syn multimers on exocellular vesicles can be more effectively absorbed by neighboring cells, facilitating their spread (*43*). The close association of multimers with membranes may be crucial in the context of the long-distance of α-syn on exocellular vesicles. However, the number of self-limiting multimers on each vesicle is tightly controlled, which likely represents a measure to prevent pathological buildup. This regulation maintains the stability of membrane-bound multimers in regions that are devoid of α-syn (*46*), promoting efficient intercellular transport while mitigating the risk of pathological outcomes of uncontrolled α-syn multimerization and aggregation. Under diseased circumstances, such as in the familial PD caused by the E46K mutation, this self-controlled multimerization process may be disrupted, leading to faster aggregation and fibrillation, contributing to pathology. In contrast, in the familial PD caused by Synuclein Alpha (SNCA) gene duplication or

triplication (*65*), two- to threefold increase of α-syn protein concentration may not disturb this self-controlled process but influence the latter steps of pathological aggregation process.

Single-molecule tracking of α-syn on membranes revealed occasional trapping, likely at sites of imperfections in lipid packing, which is crucial for the stabilization of membrane interactions. These trapping events lead to more stable adsorption of monomers onto the lipid bilayer. The movements of α-syn into and out of these trapping zones indicate that they result from transient fluctuations in membrane lipids, rather than from defects in the preparation of the experimental lipid bilayer. These imperfections may attract protein components, such as the N-terminal helix of α-syn, which has an affinity for specific conformations. We speculate that the formation and occupation of trapping sites by multimers reduce the likelihood of monomer trapping nearby owing to the weak interactions being left between α-syn monomers and defect-free membranes. This results in large gaps between the multimers and a limited density of multimers, dictated by the availability of trapping sites. The correlation between low multimer density and membrane packing defects is plausible. Vanni *et al.* (*58*) suggest that defects larger than 10 to 15 $Å^2$ enhance binding of proteins with specific lipid packing sensor motifs. The observed distances between α-syn multimers in our study are consistent with these findings. Although directly observing these defects is challenging, increased adsorption of α-syn on liposomes undergoing certain changes supports this hypothesis. The existence of local trapping sites substantially extends α-syn's dwell time on the membrane, contrasting with its relatively weak binding in areas free of traps. This phenomenon has important implications for α-syn's functional and pathological interactions with cellular membranes. The sparse multimers and their self-limited growth help moderate α-syn accumulation on membranes.

Although single-molecule imaging has been shown to be a powerful tool for the study of protein-membrane interactions, the method has some limitations. In vitro studies generally require the use of purified proteins, and most membrane proteins require encapsulation with detergents, because of their hydrophobicity, and this can adversely affect the study of membrane interactions. Membrane proteins need to be processed, for example, recombining them onto liposomes. In this study, α-syn has a disordered structure in aqueous solution and good water solubility, making it more suitable for single-molecule imaging. Owing to the bleaching effect of the fluorescent molecule, imaging can only be performed for a relatively short period, and therefore, it is necessary to be aware of any resulting biases in the data. The rapid development of photostable fluorescent probes (*66*) may help to overcome this challenge by extending the time available for observations to be made. Last, although they are important in regulating protein-membrane interactions, lipid packing imperfections are currently difficult to observe directly by means of single-molecule fluorescence experiments, but improvements in the method may be made in the future.

In conclusion, in the present study, we have revealed the intricate dynamics of α-syn multimerization on lipid bilayers. This work provides a detailed perspective regarding the self-limiting multimerization of α-syn on lipid membranes at the single-molecule level and has thereby identified complexities that would not be apparent in bulk experiments. We have made several key findings: (i) α-Syn has a notably low tendency to occupy liposome surfaces but forms stable multimers on their surfaces, even at low concentrations. (ii) Although α-syn quickly forms multimers when it binds to lipid bilayers, the expansion of these multimers is stringently controlled, representing a regulatory mechanism that prevents excessive multimerization, which is associated with a high risk of pathological amyloid aggregation. (iii) Despite the presence of numerous monomers and very dense negatively charged lipids, there are substantial gaps on the surfaces between the membrane-bound α-syn multimers, suggesting that there is precise regulation of their spatial arrangement. (iv) The dynamic interaction within α-syn multimers on lipid bilayers hints at a self-confined mechanism that maintains multimer size. (v) The E46K and E35K mutants, in contrast to WT α-syn, tends to form larger multimers and shows greater aggregation in the presence of liposomes, which implies that these mutations may disrupt normal α-syn multimerization on membranes and enhance amyloid fibrillation in diseased states.

MATERIALS AND METHODS

Materials

All lipids in this work were purchased from Avanti Polar Lipids Inc., including DOPC, DOPA, and 1,2-dipalmitoyl-*sn*-glycero-3-phosphoethanolamine-*N*-(cap biotinyl) (biotin-PE). The mini extruder and its accessories for the preparation of the liposomes were also from Avanti Polar Lipids Inc.

The coverslips were from Thermo Fisher Scientific, and the reagents used for buffer preparation and modifying the surface were mainly from Merck, including disodium hydrogen phosphate (Na_2HPO_4), sodium phosphate monobasic (NaH_2PO_4), sodium chloride (NaCl), acetone (≥99.5%), methanol (high-performance liquid chromatography grade), sulfuric acid (95.0 to 98.0%), hydrogen peroxide (30% solution), (3-aminopropyl) triethoxysilane (APTES; ≥99.5%), and acetic acid (99.5%). Reactive PEG derivatives, including methoxypolyethylene glycol–succinimidyl valerate (mPEG-SVA) and biotin-PEG-SVA, were bought from LaysanBio Inc.

Protein purification and labeling

Human α-syn WT and mutant gene were cloned into pET22b vector and transformed into *Escherichia coli* strain BL21 (DE3). To purify the overexpressed protein, bacterial pellets were lysed. The lysates were heated for 10 min at 100°C followed by centrifugation and then were further incubated with streptomycin (20 mg/ml) on ice for 30 min. After centrifugation, the pH value of supernatants was adjusted to 3.5. After buffer exchange, the dialyzed sample was further purified by anion exchange column (HiTrap Q FF, GE Healthcare), followed by a size exclusion chromatography (GE Healthcare, Superdex 75). The purified α-syn mutant proteins were conjugated with Alexa 555 C2 maleimide (A20346, Invitrogen) by following the user manual. After conjugation reaction, α-syn–Alexa 555 conjugates were further purified by a size exclusion chromatography (GE Healthcare, Superdex 75). The final protein concentration was measured by Bicinchoninic Acid (BCA) protein assay. The labeling rate was determined to be ~80% by measuring the concentration of Alexa 555 with fluorescence spectrometer.

Liposome preparation

The liposomes in this work were prepared by a standard extrusion method. The lipids (90% DOPC, 10% DOPA, and biotin-PE as

needed) were dissolved in chloroform/methanol (2:1, volume ratio) and mixed in a glass tube. Then, the organic solvent in the tube was evaporated in a vacuum pump, resulting in a thin lipid layer at the wall of the tube. Buffer was then added, and the tube was shaken for 60 min to make the turbid suspension of multilamellar liposomes. The liquid was transferred to plastic tubes, underwent five cycles of freeze-thawing in liquid nitrogen and 37°C, and lastly passed through the 200-nm-pore polycarbonate membranes, yielding homosized unilamellar liposomes.

Coverslip modification

The coverslips were first cleaned in acetone or methanol for 30 min and then treated by a mixture of sulfuric acid and 30% hydrogen peroxide (7:3 volume ratio) for 120 min at 95°C. The coverslip could be rinsed for SLB preparation. For liposome anchoring, the coverslips were further treated in a 5% solution of APTES in methanol. After drying, a mixture of 99% mPEG-SVA and 1% biotin-PEG-SVA was added onto each coverslip and incubated for 120 min. The coverslips were then rinsed and assembled into flow chambers.

SLB preparation

The SLB was prepared through liposome rupture on hydrophilic surface. The liposomes were added into the flow chamber and subsequently incubated overnight at 37°C. After washing with buffer to remove excess unruptured liposomes, the SLB was ready for subsequent experiments.

α-Syn binding to liposomes or SLB

In the experiments that α-syn binds to SLBs, the prepared SLB was washed with a buffer [20 mM phosphate buffer (pH 7.4) and 150 mM NaCl] to remove unruptured liposomes. α-Syn was then added, and images were recorded. In the experiments involving α-syn–liposome interactions, streptavidin was added at 0.01 mg/ml to the chamber assembled with biotin-PEG–modified coverslip. After 10-min incubation, the chamber was washed with buffer. Liposomes containing biotin-PE were then added to anchor onto the surface. α-Syn was then added to interact with the liposomes. Each of the liposome or SLB binding experiments were repeated at least three times to ensure the reliability.

ThT fluorescence assay for aggregation of α-syn

α-Syn WT, E46K, and E35K mutant proteins (monomer) and liposomes were prepared as described above. α-Syn WT (100 μM) and mutants were incubated with or without 250 μM liposomes in 50 mM tris-HCl, 150 mM KCl (pH 7.5), 0.02% NaN_3, and 50 μM ThT buffer. Reactions were performed in a black 384-well optimal bottom plate (Thermo Fisher Scientific, 142761), orbitally shaking at 37°C, 700 rpm. The ThT fluorescence signals were monitored by a BMG FLUOstar Omega plate reader using 440-nm excitation wavelength and 485-nm emission wavelength.

Negative staining transmission electron microscopy

Five microliters of ThT products was incubated on a 200-mesh glow-discharged copper grid for 45 s. The grid was then washed with double-distilled water and stained with 2% (w/v) uranyl acetate for another 45 s, followed by air drying. The samples were imaged using a Tecnai T12 transmission electron microscope (FEI) operated at 120 kV.

Data processing and statistical analysis

For fluorescence intensity analysis, the intensity profile of the recorded fluorescent spots was fitted by two-dimensional Gaussian function, and the function was integrated to represent the intensity value. For motion analysis of the proteins on SLB, the spots were fitted and localized frame wisely. The spots adjacent to each other in neighbor frames were linked to get the trajectories of the motion of the proteins, which were subsequently used for step size and dwell time analysis.

Supplementary Materials

This PDF file includes:

Supplementary Text
Figs. S1 to S9

REFERENCES AND NOTES

1. D. E. Mor, S. E. Ugras, M. J. Daniels, H. Ischiropoulos, Dynamic structural flexibility of α-synuclein. *Neurobiol. Dis.* **88**, 66–74 (2016).
2. J. Burré, M. Sharma, T. C. Südhof, Cell biology and pathophysiology of α-synuclein. *Cold Spring Harb. Perspect. Med.* **8**, a024091 (2018).
3. C. C. Jao, B. G. Hegde, J. Chen, I. S. Haworth, R. Langen, Structure of membrane-bound α-synuclein from site-directed spin labeling and computational refinement. *Proc. Natl. Acad. Sci. U.S.A.* **105**, 19666–19671 (2008).
4. D. F. Ma, C. H. Xu, W. Q. Hou, C. Y. Zhao, J. B. Ma, X. Y. Huang, Q. Jia, L. Ma, J. Diao, C. Liu, M. Li, Y. Lu, Detecting single-molecule dynamics on lipid membranes with quenchers-in-a-liposome FRET. *Angew. Chem. Int. Ed. Engl.* **58**, 5577–5581 (2019).
5. T. S. Ulmer, A. Bax, N. B. Cole, R. L. Nussbaum, Structure and dynamics of micelle-bound human α-synuclein. *J. Biol. Chem.* **280**, 9595–9603 (2005).
6. A. R. Braun, M. M. Lacy, V. C. Ducas, E. Rhoades, J. N. Sachs, α-Synuclein's uniquely long amphipathic helix enhances its membrane binding and remodeling capacity. *J. Membr. Biol.* **250**, 183–193 (2017).
7. E. R. Georgieva, T. F. Ramlall, P. P. Borbat, J. H. Freed, D. Eliezer, Membrane-bound α-synuclein forms an extended helix: Long-distance pulsed ESR measurements using vesicles, bicelles, and rodlike micelles. *J. Am. Chem. Soc.* **130**, 12856–12857 (2008).
8. D.-F. Ma, V. W. Q. Hou, C.-H. Xu, C.-Y. Zhao, J.-B. Ma, X.-Y. Huang, Q. Jia, L. Ma, C. Liu, M. Li, Y. Lu, Investigation of structure and dynamics of α-synuclein on membrane by quenchers-in-a-liposome fluorescence resonance energy transfer method. *Acta Phys. Sin.* **69**, 038701 (2020).
9. G. Fusco, A. De Simone, T. Gopinath, V. Vostrikov, M. Vendruscolo, C. M. Dobson, G. Veglia, Direct observation of the three regions in α-synuclein that determine its membrane-bound behaviour. *Nat. Commun.* **5**, 3827 (2014).
10. J. Burré, M. Sharma, T. C. Südhof, α-Synuclein assembles into higher-order multimers upon membrane binding to promote SNARE complex formation. *Proc. Natl. Acad. Sci. U.S.A.* **111**, E4274–E4283 (2014).
11. H. A. Lashuel, C. R. Overk, A. Oueslati, E. Masliah, The many faces of α-synuclein: From structure and toxicity to therapeutic target. *Nat. Rev. Neurosci.* **14**, 38–48 (2013).
12. P. Calabresi, G. Di Lazzaro, G. Marino, F. Campanelli, V. Ghiglieri, Advances in understanding the function of alpha-synuclein: Implications for Parkinson's disease. *Brain* **146**, 3587–3597 (2023).
13. V. Gao, J. A. Briano, L. E. Komer, J. Burré, Functional and pathological effects of α-synuclein on synaptic SNARE complexes. *J. Mol. Biol.* **435**, 167714 (2023).
14. J. Sun, L. Wang, H. Bao, S. Premi, U. Das, E. R. Chapman, S. Roy, Functional cooperation of α-synuclein and VAMP2 in synaptic vesicle recycling. *Proc. Natl. Acad. Sci. U.S.A.* **116**, 11113–11115 (2019).
15. J. Diao, J. Burré, S. Vivona, D. J. Cipriano, M. Sharma, M. Kyoung, T. C. Südhof, A. T. Brunger, Native α-synuclein induces clustering of synaptic-vesicle mimics via binding to phospholipids and synaptobrevin-2/VAMP2. *eLife* **2**, e00592 (2013).
16. G. Fusco, T. Pape, A. D. Stephens, P. Mahou, A. R. Costa, C. F. Kaminski, G. S. Kaminski Schierle, M. Vendruscolo, G. Veglia, C. M. Dobson, A. De Simone, Structural basis of synaptic vesicle assembly promoted by α-synuclein. *Nat. Commun.* **7**, 12563 (2016).
17. B. Cai, J. Liu, Y. Zhao, X. Xu, B. Bu, D. Li, L. Zhang, W. Dong, B. Ji, J. Diao, Single-vesicle imaging quantifies calcium's regulation of nanoscale vesicle clustering mediated by α-synuclein. *Microsyst. Nanoeng.* **6**, 38 (2020).
18. Y. Lai, C. Zhao, Z. Tian, C. Wang, J. Fan, X. Hu, J. Tu, T. Li, J. Leitz, R. A. Pfuetzner, Z. Liu, S. Zhang, Z. Su, J. Burré, D. Li, T. C. Südhof, Z.-J. Zhu, C. Liu, A. T. Brunger, J. Diao, Neutral lysophosphatidylcholine mediates α-synuclein-induced synaptic vesicle clustering. *Proc. Natl. Acad. Sci. U.S.A.* **120**, e2310174120 (2023).

19. G. Bellomo, C. M. G. De Luca, F. P. Paoletti, L. Gaetani, F. Moda, L. Parnetti, α-synuclein seed amplification assays for diagnosing synucleinopathies: The way forward. *Neurology* **99**, 195–205 (2022).
20. M. X. Henderson, J. Q. Trojanowski, V. M. Lee, α-synuclein pathology in Parkinson's disease and related α-synucleinopathies. *Neurosci. Lett.* **709**, 134316 (2019).
21. F. Cheng, G. Vivacqua, S. Yu, The role of alpha-synuclein in neurotransmission and synaptic plasticity. *J. Chem. Neuroanat.* **42**, 242–248 (2011).
22. J. M. Beitz, Parkinson's disease: A review. *Front. Biosci.* **6**, 65–74 (2014).
23. E. Tolosa, A. Garrido, S. W. Scholz, W. Poewe, Challenges in the diagnosis of Parkinson's disease. *Lancet Neurol.* **20**, 385–397 (2021).
24. P. Kumari, D. Ghosh, A. Vanas, Y. Fleischmann, T. Wiegand, G. Jeschke, R. Riek, C. Eichmann, Structural insights into α-synuclein monomer-fibril interactions. *Proc. Natl. Acad. Sci. U.S.A.* **118**, e2012171118 (2021).
25. A. Sokratian, J. Ziaee, K. Kelly, A. Chang, N. Bryant, S. Wang, E. Xu, J. Y. Li, S. H. Wang, J. Ervin, S. M. Swain, R. A. Liddle, A. B. West, Heterogeneity in α-synuclein fibril activity correlates to disease phenotypes in Lewy body dementia. *Acta Neuropathol.* **141**, 547–564 (2021).
26. D. Li, C. Liu, Conformational strains of pathogenic amyloid proteins in neurodegenerative diseases. *Nat. Rev. Neurosci.* **23**, 523–534 (2022).
27. Y. Li, C. Zhao, F. Luo, Z. Liu, X. Gui, Z. Luo, X. Zhang, D. Li, C. Liu, X. Li, Amyloid fibril structure of α-synuclein determined by cryo-electron microscopy. *Cell Res.* **28**, 897–903 (2018).
28. D. Li, C. Liu, Molecular rules governing the structural polymorphism of amyloid fibrils in neurodegenerative diseases. *Structure* **31**, 1335–1347 (2023).
29. C. M. Dobson, T. P. J. Knowles, M. Vendruscolo, The amyloid phenomenon and its significance in biology and medicine. *Cold Spring Harb. Perspect. Biol.* **12**, a033878 (2020).
30. D. Eisenberg, M. Jucker, The amyloid state of proteins in human diseases. *Cell* **148**, 1188–1203 (2012).
31. A. P. Pandey, F. Haque, J. C. Rochet, J. S. Hovis, Clustering of α-synuclein on supported lipid bilayers: Role of anionic lipid, protein, and divalent ion concentration. *Biophys. J.* **96**, 540–551 (2009).
32. M. Grey, C. J. Dunning, R. Gaspar, C. Grey, P. Brundin, E. Sparr, S. Linse, Acceleration of α-synuclein aggregation by exosomes. *J. Biol. Chem.* **290**, 2969–2982 (2015).
33. M. S. Terakawa, Y. Lin, M. Kinoshita, S. Kanemura, D. Itoh, T. Sugiki, M. Okumura, A. Ramamoorthy, Y. H. Lee, Impact of membrane curvature on amyloid aggregation. *Biochim. Biophys. Acta Biomembr.* **1860**, 1741–1764 (2018).
34. C. Zhao, J. Tu, C. Wang, W. Liu, J. Gu, Y. Yin, S. Zhang, D. Li, J. Diao, Z.-J. Zhu, C. Liu, Lysophosphatidylcholine binds α-synuclein and prevents its pathological aggregation. *Natl. Sci. Rev.* **11**, nwae182 (2024).
35. V. Gilmozzi, G. Gentile, M. P. Castelo Rueda, A. A. Hicks, P. P. Pramstaller, A. Zanon, M. Lévesque, I. Pichler, Interaction of alpha-synuclein with lipids: Mitochondrial cardiolipin as a critical player in the pathogenesis of Parkinson's disease. *Front. Neurosci.* **14**, 578993 (2020).
36. T. Ryan, V. V. Bamm, M. G. Stykel, C. L. Coackley, K. M. Humphries, R. Jamieson-Williams, R. Ambasudhan, D. D. Mosser, S. A. Lipton, G. Harauz, S. D. Ryan, Cardiolipin exposure on the outer mitochondrial membrane modulates α-synuclein. *Nat. Commun.* **9**, 817 (2018).
37. S. Ghio, F. Kamp, R. Cauchi, A. Giese, N. Vassallo, Interaction of α-synuclein with biomembranes in Parkinson's disease—role of cardiolipin. *Prog. Lipid Res.* **61**, 73–82 (2016).
38. J. Galper, N. J. Dean, R. Pickford, S. J. G. Lewis, G. M. Halliday, W. S. Kim, N. Dzamko, Lipid pathway dysfunction is prevalent in patients with Parkinson's disease. *Brain* **145**, 3472–3487 (2022).
39. E. Sinclair, D. K. Trivedi, D. Sarkar, C. Walton-Doyle, J. Milne, T. Kunath, A. M. Rijs, R. M. A. de Bie, R. Goodacre, M. Silverdale, P. Barran, Metabolomics of sebum reveals lipid dysregulation in Parkinson's disease. *Nat. Commun.* **12**, 1592 (2021).
40. J. Zhang, Q. Liu, Cholesterol metabolism and homeostasis in the brain. *Protein Cell* **6**, 254–264 (2015).
41. M. Fais, A. Dore, M. Galioto, G. Galleri, C. Crosio, C. Iaccarino, Parkinson's disease-related genes and lipid alteration. *Int. J. Mol. Sci.* **22**, 7630 (2021).
42. I. F. Tsigelny, Y. Sharikov, V. L. Kouznetsova, J. P. Greenberg, W. Wrasidlo, C. Overk, T. Gonzalez, M. Trejo, B. Spencer, K. Kosberg, E. Masliah, Molecular determinants of α-synuclein mutants' oligomerization and membrane interactions. *ACS Chem. Neurosci.* **6**, 403–416 (2015).
43. K. M. Danzer, L. R. Kranich, W. P. Ruf, O. Cagsal-Getkin, A. R. Winslow, L. Zhu, C. R. Vanderburg, P. J. McLean, Exosomal cell-to-cell transmission of alpha synuclein oligomers. *Mol. Neurodegener.* **7**, 42 (2012).
44. M. Guo, J. Wang, Y. Zhao, Y. Feng, S. Han, Q. Dong, M. Cui, K. Tieu, Microglial exosomes facilitate α-synuclein transmission in Parkinson's disease. *Brain* **143**, 1476–1497 (2020).
45. S. Neupane, E. De Cecco, A. Aguzzi, The hidden cell-to-cell trail of α-Synuclein aggregates. *J. Mol. Biol.* **435**, 167930 (2023).
46. G. C. Hassink, C. C. Raiss, I. M. J. Segers-Nolten, R. J. A. van Wezel, V. Subramaniam, J. le Feber, M. M. A. E. Claessens, Exogenous α-synuclein hinders synaptic communication in cultured cortical primary rat neurons. *PLOS ONE* **13**, e0193763 (2018).
47. K. K. Kumar, H. Wang, C. Habrian, N. R. Latorraca, J. Xu, E. S. O'Brien, C. Zhang, E. Montabana, A. Koehl, S. Marqusee, E. Y. Isacoff, B. K. Kobilka, Stepwise activation of a metabotropic glutamate receptor. *Nature* **629**, 951–956 (2024).
48. W. B. Asher, P. Geggier, M. D. Holsey, G. T. Gilmore, A. K. Pati, J. Meszaros, D. S. Terry, S. Mathiasen, M. J. Kaliszewski, M. D. McCauley, A. Govindaraju, Z. Zhou, K. G. Harikumar, K. Jaqaman, L. J. Miller, A. W. Smith, S. C. Blanchard, J. A. Javitch, Single-molecule FRET imaging of GPCR dimers in living cells. *Nat. Methods* **18**, 397–405 (2021).
49. J. Diao, Z. Su, Y. Ishitsuka, B. Lu, K. S. Lee, Y. Lai, Y. K. Shin, T. Ha, A single-vesicle content mixing assay for SNARE-mediated membrane fusion. *Nat. Commun.* **1**, 54 (2010).
50. C. Yang, X. He, H. Wang, Z. Lin, W. Hou, Y. Lu, S. Hu, M. Li, Single-molecule monitoring of membrane association of the necroptosis executioner MLKL with discernible anchoring and insertion dynamics. *Nano Lett.* **23**, 4770–4777 (2023).
51. D. Ma, W. Hou, C. Yang, S. Hu, W. Han, Y. Lu, Real-time imaging of structure and dynamics of transmembrane biomolecules by FRET-induced single-molecule fluorescence attenuation. *Biophys. Rep.* **7**, 490–503 (2021).
52. N. Kučerka, E. Ermakova, E. Dushanov, K. T. Kholmurodov, S. Kurakin, K. Želinská, D. Uhríková, Cation-zwitterionic lipid interactions are affected by the lateral area per lipid. *Langmuir* **37**, 278–288 (2021).
53. M. Giménez-Andrés, A. Čopič, B. Antonny, The many faces of amphipathic helices. *Biomolecules* **8**, 45 (2018).
54. J. Bigay, B. Antonny, Curvature, lipid packing, and electrostatics of membrane organelles: Defining cellular territories in determining specificity. *Dev. Cell* **23**, 886–895 (2012).
55. G. Fuertes, D. Giménez, S. Esteban-Martin, A. J. Garcia-Sáez, O. Sánchez, J. Salgado, Role of membrane lipids for the activity of pore forming peptides and proteins. *Adv. Exp. Med. Biol.* **677**, 31–55 (2010).
56. R. Gautier, A. Bacle, M. L. Tiberti, P. F. Fuchs, S. Vanni, B. Antonny, Packmem: A versatile tool to compute and visualize interfacial packing defects in lipid bilayers. *Biophys. J.* **115**, 436–444 (2018).
57. J. Liu, B. Bu, M. Crowe, D. Li, J. Diao, B. Ji, Membrane packing defects in synaptic vesicles recruit complexin and synuclein. *Phys. Chem. Chem. Phys.* **23**, 2117–2125 (2021).
58. S. Vanni, H. Hirose, H. Barelli, B. Antonny, R. Gautier, A sub-nanometre view of how membrane curvature and composition modulate lipid packing and protein recruitment. *Nat. Commun.* **5**, 4916 (2014).
59. W. Choi, S. Zibaee, R. Jakes, L. C. Serpell, B. Davletov, R. A. Crowther, M. Goedert, Mutation E46K increases phospholipid binding and assembly into filaments of human α-synuclein. *FEBS Lett.* **576**, 363–368 (2004).
60. K. Zhao, Y. Li, Z. Liu, H. Long, C. Zhao, F. Luo, Y. Sun, Y. Tao, X. D. Su, D. Li, X. Li, C. Liu, Parkinson's disease associated mutation E46K of α-synuclein triggers the formation of a distinct fibril structure. *Nat. Commun.* **11**, 2643 (2020).
61. J. J. Zarranz, J. Alegre, J. C. Gómez-Esteban, E. Lezcano, R. Ros, I. Ampuero, L. Vidal, J. Hoenicka, O. Rodriguez, B. Atarés, V. Llorens, E. Gomez Tortosa, T. del Ser, D. G. Muñoz, J. G. de Yebenes, The new mutation, E46K, of α-synuclein causes parkinson and Lewy body dementia. *Ann. Neurol.* **55**, 164–173 (2004).
62. B. Winner, R. Jappelli, S. K. Maji, P. A. Desplats, L. Boyer, S. Aigner, C. Hetzer, T. Loher, M. Vilar, S. Campioni, C. Tzitzilonis, A. Soragni, S. Jessberger, H. Mira, A. Consiglio, E. Pham, E. Masliah, F. H. Gage, R. Riek, In vivo demonstration that alpha-synuclein oligomers are toxic. *Proc. Natl. Acad. Sci. U.S.A.* **108**, 4194–4199 (2011).
63. M. M. Wördehoff, W. Hoyer, α-synuclein aggregation monitored by Thioflavin T fluorescence assay. *Bio Protoc.* **8**, e2941 (2018).
64. A. I. Sulatskaya, N. P. Rodina, M. I. Sulatsky, O. I. Povarova, I. A. Antifeeva, I. M. Kuznetsova, K. K. Turoverov, Investigation of α-synuclein amyloid fibrils using the fluorescent probe thioflavin T. *Int. J. Mol. Sci.* **19**, 2486 (2018).
65. H. Deng, L. Yuan, Genetic variants and animal models in SNCA and Parkinson disease. *Ageing Res. Rev.* **15**, 161–176 (2014).
66. Y. Zhang, C. Yang, S. Peng, J. Ling, P. Chen, Y. Ma, W. Wang, Z. Chen, C. Chen, General strategy to improve the photon budget of thiol-conjugated cyanine dyes. *J. Am. Chem. Soc.* **145**, 4187–4198 (2023).

Acknowledgments

Funding: This work was supported by the National Key R&D Program of China (2019YFA0709304), the National Natural Science Foundation of China (T2221001, 12090051, 11974411, 12022409, 92353302, 32171236, 32170683, and 82188101), the Guangdong Basic and Applied Basic Research Foundation (2020A1515110102), the Strategic Priority Research Program of the Chinese Academy of Sciences (XDB0480000), the Science and Technology Commission of Shanghai Municipality (STCSM) (20XD1425000, 2019SHZDZX02, and 22JC1410400), the CAS project for Young Scientists in Basic research (YSBR-095), the Shanghai Pilot Program for Basic Research–Chinese Academy of Science Shanghai Branch (CYJ-SHFY-2022-005), and the China Postdoctoral Science Foundation (2020 M680728). **Author contributions:** Conceptualization: C.L., M.L., and Y.L. Data curation: D.-F.M. and Z.H. Formal

analysis: D.-F.M., S.-Y.X., and Shengnan Zhang. Funding acquisition: M.L., Y.L., C.L., and D.-F.M. Investigation: D.-F.M., S.-Y.X., Shenqing Zhang, Z.H., D.L., Y.T., and F.C. Methodology: C.L., D.-F.M., S.-Y.X., Shenqing Zhang, Z.H., Shengnan Zhang, D.L., Y.T., and F.C. Project administration: M.L. and Y.L. Resourses: D.-F.M. and Shenqing Zhang. Supervision: C.L., M.L., and Y.L. Validation: D.-F.M., S.-Y.X., and Shenqing Zhang. Visualization: D.-F.M. and Shengnan Zhang. Writing—original draft: D.-F.M., C.L., and T.C. Writing—review and editing: C.L., M.L., Y.L., D.-F.M., Shengnan Zhang, and T.C. **Competing interests:** The authors declare that they have no competing interests. **Data and materials availability:** All data needed to evaluate the conclusions in the paper are present in the paper and/or the Supplementary Materials.

Submitted 5 February 2024
Accepted 4 September 2024
Published 9 October 2024
10.1126/sciadv.ado4893